A Detailed Reaction Kinetic Model of Light Naphtha Isomerization on Pt/zeolite Catalyst

Zaidoon M. Shakor [a], María Jesús Ramos[b], Adnan A. Abdul Razak[a]*

a Department of Chemical Engineering, University of Technology, Iraq.

b Departamento de Ingeniería Química, Facultad de Ciencias Químicas, Universidad de Castilla-La Mancha, Avd. Camilo José Cela s/n, 13071 Ciudad Real, Spain.

* Corresponding author. Email: 80036@uotchnology.edu.iq

Abstract

There is both a practical and theoretical interest in creating accurate kinetic models of catalytic refining processes, as these models can be used to improve refining methods. Such models can predict process performance, such as process configuration, recycling some streams, and determining optimal operating conditions. In this work, a detailed reaction kinetic model was developed to describe light naphtha isomerization reactions over different Pt/zeolite catalysts (i.e., Pt/mordenite, Pt/ZSM5, and Pt/BETA). The proposed kinetic model involved 117 isomerization reactions and 90 cracking reactions for 52 real light naphtha components graded from methane to n-octane. A power law reaction kinetic was assumed for all reactions, and 414 kinetic parameters were fine-tuned by benchmarking the finding model with the experimental results of light naphtha isomerization obtained at six temperatures (i.e., 290, 310, 330, 350, 370, and 390°C). All computations in the present study were done using the genetic algorithm stochastic optimization method coded by MATLAB 2015a software to estimate the optimum set of kinetic parameters. The mean absolute error for all component compositions at various temperatures was found to be 0.003608, 0.004841, and 0.004757 for Pt/mordenite, Pt/ZSM5, and Pt/BETA catalysts, respectively.

Keywords: kinetic model; light naphtha; isomerization; genetic algorithm.

1. Introduction

Isomerization is one of the most effective processes in the modern petroleum refinery to upgrade light naphtha by increasing its isomer and aromatic composition. A light naphtha isomerization unit has economic benefits and also protects the environment by minimizing the amount of harmful gases, such as carbon dioxide and nitrous oxide, emitted into the atmosphere [1]. As the petroleum industry moved toward marketing fuels with lower lead levels, it became increasingly difficult to use light straight run naphtha in the gasoline pool. Conversion of the low octane C5/C6 normal paraffins to their corresponding branched isomers to increase their octane number is recognized as a logical and necessary step in a lead reduction program [2].

Each component within the light naphtha unit had an octane number different than the others, and the normal paraffins also had octane numbers lower than the isomers. The octane number of light naphtha components was graded from 0 for n-heptane to 112.1 for 2,2,3-trimethylbutane. Therefore, designing and selecting the operating conditions for a light naphtha isomerization unit required a highly accurate reaction kinetic model to properly estimate the product composition [3]. Typically, the octane number of light naphtha is within the range from 60-70 RONs, depending on the origin of the crude oil feed and the cut point within the distillation column. A light naphtha isomerization unit provides an octane boost of 15-30 points, depending on the flow scheme, feed type, and catalysts [4].

Ideally, the isomerization catalyst would convert the feed paraffins to the highest octane number branched structure (i.e., normal pentane to iso-pentane, and normal hexane to 2,2-dimethylbutane or 2,3-dimethylbutane). However, using low reaction temperatures during isomerization prevents cracking reactions [5]. Many studies have been conducted in the past few years on the isomerization of n-alkanes: n-butane [6-8], n-hexane [9-13], n-heptane [14-17], and n-octane [18-21].

Although the alkane hydroisomerization literature deals with zeolites loaded with many metals (i.e., Co, Fe, Ir, Ni, Pt, Pd, Re, Rh, Ru, and Zn), Pt/zeolites were found to be more selective toward isomers and also more stable. Zeolites are crystallized silico-aluminates that are used to make a catalyst more acidic. Metallic particles of platinum are impregnated on the surface of zeolites and act as hydrogen transfer centers [22-25]. In industrial isomerization units, three metal-acid catalysts are widely used (i.e., Pt/chlorinated alumina, sulfated zirconia (SZr), and Pt/zeolite), and their selection depends on the process characteristics and feed stock properties. Chlorinated catalysts are very sensitive to all types of contaminants in the feedstock,

while zeolite- based catalysts can tolerate sulfur and water in the feed. Chlorided alumina catalysts usually operate at lower temperatures, in the range of 130-170ºC, and thus, do not have thermodynamic limitations on their isomerization reactions. Zeolite-based catalysts are very robust and operate commercially at sulfur levels exceeding 100 ppm in naphtha feedstock and at temperatures ranging from 250-350ºC.

Although there are dozens of studies dealing with kinetic models of isomerization reactions for individual light naphtha components, there has been little research to predict a kinetic model for the isomerization process of light naphtha. Faskhutdinov et al. (2019) used a three-reactor block to study the transformation of C5 and C6 fractions in the catalytic isomerization process. A kinetic model of the process was built, and 102 kinetic parameters were determined [26].

Hayati et al. (2014) developed a reaction network for light naphtha isomerization including 15 lumps and 16 reactions. Isomerization, saturation, ring opening, and hydrocracking reactions were taken into consideration. They investigated the influence of hydrocracking reactions as well as other reactions on the research octane number (RON) of the isomerization product, finding that when other process variables (i.e., the hydrogen-to-feed molar ratio and liquid hourly space velocity [LHSV]) were kept constant, increasing the reactor temperature increased the RON of the product [27].

Chekantsev et al. (2014) proposed a universal kinetic model for the industrial isomerization unit of light naphtha. The feed consisted of C5/C6, while C7+ was aggregated due to the trace number of hydrocarbons being heavier than the C7 in the feed. The reactor was considered an ideal plug flow. Kinetic parameters were defined for $Pt/Al_2O_3–CCl_4$, Pt/zeolite, and $Pt/SO_4–ZrO_2$ catalysts for the reaction scheme of 36 reactions and 36 components [28].

Cheng et al. (1991) proposed a simplified network form of n-hexane isomerization over Pt/HM and Pd/Al_2O_3 catalysts. The rate constants were calculated using the two-point method [29]. Koncsag et al. (2011) studied the isomerization of C5/C6 on Pt/H-zeolite in an industrial plug flow reactor. The kinetic parameters of the main isomerization reactions were found. The kinetic model was valid for the range of parameters under the test conditions [30].

Chen et al. (2015) developed a 22-lump kinetic model for fluid catalytic cracking naphtha hydroisomerization and estimated the model's kinetic parameters. From the experimental results, they observed that the main reactions that occurred were dimerization, cracking, isomerization, and aromatization of olefins [31]. Ahmed et al. (2018) developed a detailed process model for an industrial naphtha isomerization unit and estimated the kinetic parameters of 36 reactions within the proposed kinetic model by minimizing the sum of squared errors between the experimental data and the predicted results [32].

Hidalgo et al. (2004) studied C5-C7 paraffin isomerization over a Pt/WO3–ZrO2 catalyst using an industrial feedstock. Experiments were carried out under various operating conditions to optimize the reaction at 250 and 300^{o}C [33].

Due to the lack of experimental data in the field of light naphtha isomerization, the experimental results used in the present study were taken from [23] because they investigated industrial light naphtha feedstock using three catalysts and six temperatures (from 290^{o}C to 390^{o}C), which provided validity for the proposed kinetic model. Most of the previous models [27-32], while simplified, are also detailed in relation to specific catalysts and the C5 and C6 feed. Hence, there was a need to develop a universal kinetic model for light naphtha isomerization reactions. This study proposed a kinetic model of the isomerization process of the real feed of light alkanes using three types of catalysts. The proposed mechanism reaction

involved isomerization and hydrocracking reactions. The extensive feed consisted of 52 individual compounds having carbon atoms from 1 to 8. The reaction scheme of the isomerization process that included 207 reactions was proposed on the basis of experimental data from work conducted at the pilot plant unit.

2. Experimental Data

The experimental data used in the kinetic modeling of the light naphtha isomerization reactions was taken from [23]. Ramos et al. (2007) prepared and characterized three catalysts (Pt/mordenite, Pt/BETA, and Pt/ZSM). The isomerization process of real light naphtha was conducted at a pilot plant unit over the prepared catalysts at the following conditions: temperatures ranging from 290 to 390ºC), total pressure = 10 bar, weight of the catalyst = 1.5g, weight hourly space velocity (WHSV) = 10 h^{-1}, and H_2 /HC molar ratio = 14. The data describes the composition of the feed and effluent from the reactor at different temperatures.

3. Mathematical Modeling

3.1 *Model Assumptions*

The following assumptions were considered in the mathematical modeling:

1. One-dimensional plug flow in the reactor.
2. Homogenous gas phase reactions.
3. Pseudo-first-order reactions.
4. Isothermal and non-adiabatic reactor condition.

3.2 *Proposed Reaction Kinetics*

The previous works on kinetic modeling of the light naphtha isomerization process mentioned the following reaction mechanisms: paraffin and naphthene isomerization; naphthene hydrogenation; and benzene saturation [23,32,34]. In the present work, an attempt was made to include the hydrocracking reaction of the formed products. The hydrocracking reaction depends

on the feed composition and severity of the process. Large hydrocarbon (HC) molecules crack more than smaller molecules. As the isomerization of normal paraffin C5/C6 reach equilibrium, the extent of the hydrocracking reactions increases. If the isomerization is excessive, hydrocracking occurs. As the vapor product (e.g., methane, ethane, propane, and butane) increases, the yield of the liquid decreases, and the heat of the product increases. This increases the reactor temperature and the rate of isomerization, which produces a state closer to equilibrium. At excessively high temperatures, the reaction rate will be high, and the concentration of isoparaffins in the product will decrease because of the downward shift in the equilibrium curve. If the temperature is raised more than is optimal, the hydrocracking reaction will increase without any tangible effects from other reactions. Furthermore, larger molecules have a tendency to crack more than smaller molecules. Extremely high temperatures may lead to an increased rate of carbon laydown on the catalyst; however, the carbon-forming propensity on the catalyst surface is so low that excessive hydrocracking would normally be encountered before carbon-formation problems would develop.

The kinetic model employed in this work includes 207 reactions. Table 1 shows the details of these reactions. The one-dimensional plug flow reactor hypothesis was assumed to model a fixed-bed isomerization reactor. The following differential equations were employed to represent the difference in the quantity of the components within the reactor bed:

$$\frac{dF_i}{dw} = -\sum_{j}^{m} S_{i,j} r_j \qquad (1)$$

where F_i is the molar flow rate of species i (mol/hr), w is the weight of the catalyst (g), r_j is the reaction rate per catalyst mass (mol/hr. gm), and s_{ij} is the stoichiometric coefficient for the i^{th} component participating in the j^{th} reaction.

When isomerization occurs at higher temperatures, all reactions take place in a gaseous phase. Therefore, the reaction rate equation was expressed in terms of the partial pressures of the reaction components, as shown in Eq. 2:

$$r_j = k_j P_i^o \qquad (2)$$

An Arrhenius equation was used to represent the variation in the reaction rate constants with temperature and activation energy, using the following equation:

$$k_j = k_j^o \exp\left(-\frac{E_{Aj}}{RT}\right) \qquad (3)$$

where Pi is the partial pressure (bar), R is the gas constant 8.314 (J/mol ^oK), T is the temperature (^oK), A is the pre-exponential factor (mol/gm.cat.hr bar), and E_A is the activation energy (J.mol^{-1}).

3.3 *Kinetic Parameters Estimation*

A differential evaluation optimization algorithm was used to estimate a global optimum set of kinetic parameters by minimizing the objective function (f), which represents the deviations in the composition of the reactors' effluents.

$$f = \frac{1}{n_{exp}} \sum_{i=1}^{n_{exp}} \left(\frac{1}{n_{Com}} \sum_{j=1}^{n_{Com}} \left| y_{i,j}^{exp} - y_{i,j}^{pred} \right| \right) \qquad (4)$$

The proposed model involved 53 ordinary differential equations (52 for naphtha components and one for hydrogen). A fourth-order Runge-Kutta integration method was used to solve these differential equations, which are represented in Eq. 1. All computations within this study were predicted using programs coded using MATLAB 2015a software. Genetic algorithm optimization was used to estimate the optimum set of kinetic parameters. MATLAB sub-subroutines ***ode15s*** and ***ga*** were used in integration and optimization. The values of the pre-exponential factors (A_1 to A_{207}) and the activation energies (E_1 to E_{207}) were estimated and are presented in Table 1.

[Table 1 near here]

4. Results and Discussion

4.1 *Research Octane Number*

Branched alkanes have high research octane numbers (RONs) compared to linear alkanes, and the isomerization (branching) of alkanes is a key reaction for improving the octane number of gasoline. The octane rating uses a scale where heptane is given an arbitrary score of 0 and 2,2,4-trimethylpentane (iso-octane) range is scored from one of 100. Thus, petrol with the same knocking characteristics as a mixture of 95% 2,2,4-trimethylpentane and 5% heptane has an octane rating of 95. A rating of 95 does not mean that the petrol contains only iso-octane and heptane in these proportions but that it has the same tendency to knock as this mixture.

Figure 1 shows the experimental and predicted RONs of the product at different temperatures. The RON of the isomerization product was calculated according to Eq. 5 [35]:

$$RON = \sum_{i=1}^{nc} y_i \times RON_i \qquad (5)$$

where y_i is the fraction of component i present in the isomerization product, and RONi is the RON of component i.

Based on the above results, increasing the temperature had a positive effect on the RON for all types of catalysts, where the RON of the products was 53.1, 70.8, and 72.7 compared to 41.5, 42.9, and 43.5 of the feed for mordenite, Pt/ZSM5, and Pt/BETA catalysts, respectively. It was expected that increasing the temperature would accelerate the hydrocracking reaction, which would decrease the RON of the products. However, as the temperature of the reaction increased, the RON increased due to the isomerization of the components that resulted from the cracking reaction with 5 atoms of carbon, as suggested in the previous section. According to these results,

increasing the temperature of the reaction for this type of catalyst could increase the RON from 49 to 73%. Raising the reaction temperature will increase the catalyst activity such that overall, the conversion will increase the amount of hydrocracking and hydroisomerization. The performance comparison of the three types of zeolite on the RON shows that Pt/BETA had the highest RON value because using Pt/BETA yielded a higher isomer compound compared with the other catalysts [23]. Even though the same amount of platinum (i.e., 5%) was loaded on the three different zeolites, there was a notable difference in the RON results due to variations in the pore sizes, topologies, and crystallinity of these three zeolites.

[Figure 1 near here]

4.2 *Validity of the Predictive Kinetic Model*

To prove the validity of the developed kinetic model, the predicted mole fraction was compared with the experimental data, as shown in Figure 2. It can be seen, the points cluster around the diagonal line indicates a good validity of the model, higher validity was found at higher temperatures. The absolute error between the experimental data and predicted results is very small, giving a clear indication of an excellent match between the theoretical and practical results, with a mean absolute deviation of 0.003608, 0.004841, and 0.004757 for the Pt/mordenite, Pt/ZSM5, and Pt/BETA catalysts, respectively (see Figure 3). Lower levels of error were found at higher temperatures because the proposed kinetic model included isomerization and cracking reactions, both of which were expected to occur at high temperatures. By dividing the absolute errors by the reciprocals of the number of components (52), the mean relative error based on six data sets at different temperatures (i.e., 290, 310, 330, 350, 370, and 390^{o}C) was estimated to be to 18.76%, 25.17%, and 24.74% for the Pt/mordenite, Pt/ZSM5, and Pt/BETA catalysts, respectively. Increasing the number of fitted experiments will increase the predicted error resulting from a comparison between the experimental and predicted results. But

in the present study, in spite of conducting six experiments with 52 components and three catalysts, the level of absolute error was within acceptable levels. The estimated values for the Arrhenius parameters (pre-exponential factor and activation energy) are presented in Table 1. For the isomerization of linear alkanes, a lower activation energy was observed in the forward reaction than in the reverse reaction, which explains the activity toward the isomerization of linear alkanes compared to the reverse reactions.

[Figure 2 near here]

[Figure 3 near here]

5. Conclusions

Creating an accurate kinetic model is a key step in the modeling, design, and optimization of industrial and petroleum processes. In this work, a detailed reaction kinetic model of 52 components and 207 reactions was developed to describe light naphtha isomerization reactions using three catalysts. A reaction network involves the isomerization, ring opening, benzene saturation, and hydrocracking reactions. The proposed model demonstrated the effect of cracking reactions on light naphtha isomerization using three catalysts. A comparison between the predicted mole fraction of the products and the experimental data showed a good agreement, with the mean absolute errors of 0.003608, 0.004841, and 0.004757 for the Pt/mordenite, Pt/ZSM5, and Pt/BETA catalysts, respectively.

References

1. Serra, J.M., A. Chica, and A. Corma. 2003. Development of a low temperature light paraffin isomerization catalysts with improved resistance to water and sulphur by combinatorial methods, App. Catal. A: General, 239, 35-42.

2. Dhar, A., R. L .Vekariya, and P. Sharma. 2017. Kinetics and mechanistic study of n -alkane hydroisomerization reaction on Pt-doped γ-alumina catalyst. Petroleum, 3(4), 489–495. doi:10.1016/j.petlm.2017.02.001

3. Maloncy, M. L., T. Maschmeyer, and J. C. Jansen. 2005. Technical and economical evaluation of a zeolite membrane based heptane hydroisomerization process. Chemical Engineering Journal, 106(3), 187–195. doi:10.1016/j.cej.2004.11.011

4. Shehata, W. M., M. F. Mohamed, and F. K. Gad. 2018. Monitoring and modelling of variables affecting isomerate octane number produced from an industrial isomerization process. Egyptian Journal of Petroleum. doi:10.1016/j.ejpe.2018.02.006

5. Mäki-Arvela, P., T. Kaka khel, M. Azkaar, S. Engblom, and D. Murzin. 2018. Catalytic Hydroisomerization of Long-Chain Hydrocarbons for the Production of Fuels. Catalysts, 8(11), 534. doi:10.3390/catal8110534

6. Wulfers, M. J., and F. C. Jentoft. 2015. Mechanism of n -butane skeletal isomerization on H-mordenite and Pt/H-mordenite. Journal of Catalysis, 330, 507–519. doi:10.1016/j.jcat.2014.12.035

7. Zhang, W., P. Wang, C. Yang, and C. Li. 2019. A Comparative Study of n-Butane Isomerization over H-Pt/BETA and H-ZSM-5 Zeolites at Low Temperatures: Effects of Acid Properties and Pore Structures. Catalysis Letters. doi:10.1007/s10562-019-02683-0

8. Wang, P., S. Wang, C. Yang, C. Li, X. and Bao. 2019. Effect of Aluminum Addition and Surface Moisture Content on the Catalytic Activity of Sulfated Zirconia in n-Butane Isomerization. Industrial & Engineering Chemistry Research. doi:10.1021/acs.iecr.9b01349

9. Kimura, T., J. Gao, K. Sakashita, X. Li. and S. Asaoka. 2012. Catalyst of Palladium Supported on H-Pt/BETA Zeolite with Nanosized Al2O3 for Isomerization of n-Hexane. Journal of the Japan Petroleum Institute, 551, 40–50. doi:10.1627/jpi.55.40

10. Adzamic, Z., T. Adzamic, M. Muzic, and K. Sertic-Bionda. 2013. Optimization of the n-hexane isomerization process using response surface methodology. Chemical Engineering Research and Design, 911, 100–105. doi:10.1016/j.cherd.2012.06.012

11. Pather, K., and D. Lokhat, 2014. Gas-phase Hydroisomerization of n-Hexane Over Pt/SO4-ZrO2: Kinetic Modeling and Reactor Simulation. Petroleum Science and Technology, 3223, 2786–2794. doi:10.1080/10916466.2014.903969

12. Dhar, A., N. S. Kumar, K. Sarkar, A. S. Al-Fatesh, A. A. Ibrahim, A. H. Fakeeha. and R. L. Vekariya, 2019. Acidic ionic liquids containing variable cationic head groups for catalytic isomerization of n-hexane. Journal of Molecular Liquids, 111047. doi:10.1016/j.molliq.2019.111047

13. Yang, L., Z. Song, Y. Yu, L. Zhu, and D. Xia. 2020. Bimetallic Bifunctional Pt-NiP/Hβ as a Novel and Highly Efficient Catalyst for n-Hexane Isomerization. Catalysis Surveys from Asia. doi:10.1007/s10563-020-09295-4

14. Alemán-Vázquez, L. O., J. L. Cano-Domínguez, E. Torres-García, and J. R. Villagómez-Ibarra. 2011. Industrial Aplication of Catalytic Systems for n-Heptane Isomerization. Molecules, 167, 5916–5927. doi:10.3390/molecules16075916

15. Shkurenok, V. A., M. D. Smolikov, S. S. Yablokova, D. I. Kiryanov, A. S. Belyi, E. A. Paukshtis,

16. N. N. Leonteva, T. I. Gulyaev, et al. 2015. Pt/WO3/ZrO2 Catalysts for n-Heptane Isomerization. Procedia Engineering, 113, 62–67. doi:10.1016/j.proeng.2015.07.291

17. Parsafard, N., M. H. Peyrovi, and M. Rashidzadeh. 2016. Experimental and kinetic study of n-heptane isomerization on nanoporous Pt-Re, Sn/HPT/ZSM5-HMS catalysts. Chinese Journal of Catalysis, 379, 1477–1486. doi:10.1016/s1872-20671561114-7

18. Smolikov, M. D., V. A. Shkurenok, D. I. Kir'yanov, and A. S. Belyi. 2019. Active surface formation of tungstated zirconia catalysts for n-heptane isomerization. Catalysis Today. doi:10.1016/j.cattod.2019.01.036

19. Manuale, D. L., G. C. Torres, V. M. Benítez, J. M. Badano, J. C. Yori, and J. H. Sepúlveda. 2013. Isomerization-cracking of n-octane on catalysts based on heteropolyacid H3Pw12O40 and heteropolyacid supported on zirconia and promoted with Pt and Cs. Química Nova, 367, 960–966. doi:10.1590/s0100-40422013000700007

20. Behr, A., A. Kämper, R. Kuhlmann, A. J. Vorholt, and R. Franke. 2016. First efficient catalyst recycling for the iridium-catalysed hydroformylation of 1-octene. Catalysis Science & Technology, 61, 208–214. doi:10.1039/c5cy01018g

21. Yang, Z., Y. Liu, Y. Li, L. Zeng, Z. Liu, X. Liu, and C. Liu. 2017. Effect of preparation method on the bimetallic NiCu/SAPO-11 catalysts for the hydroisomerization of n -octane. Journal of Energy Chemistry. doi:10.1016/j.jechem.2017.10.003

22. Afzali, Z., M. R. Vaezi, B. Aghabarari, and M. V. Martinez Huerta. 2019. Effect of phosphomolybdic acid on the catalytic behavior of bifunctional Pt-Cr/nanocrystalline Y zeolite in hydroisomerization of n -octane. Journal of the Chinese Chemical Society. doi:10.1002/jccs.201800475

23. Ramos, M. J., J. P. Gómez, F. Dorado, P. Sánchez, and J. L. Valverde. 2005. Hydroisomerization of a Refinery Naphtha Stream over Agglomerated Pd Zeolites. Industrial & Engineering Chemistry Research, 4424, 9050–9058. doi:10.1021/ie0507651

24. Ramos, M. J., J. P. Gómez, F. Dorado, P. Sánchez, and J. L. Valverde. 2007. Hydroisomerization of a refinery naphtha stream over platinum zeolite-based catalysts. Chemical Engineering Journal, 1261, 13–21. doi:10.1016/j.cej.2006.08.026

25. Fúnez, A., A. De Lucas, P. Sánchez, M. J. Ramos, and J. L. Valverde. 2008. Hydroisomerization in liquid phase of a refinery naphtha stream over Pt–Ni/H-Pt/BETA zeolite catalysts. Chemical Engineering Journal, 1362-3, 267–275. doi:10.1016/j.cej.2007.03.062

26. Mohammadrezaee, A., and A. Nemati Kharat. 2018. Combined light naphtha isomerization and naphthenic ring opening reaction on modified platinum on chlorinated alumina catalyst. Reaction Kinetics, Mechanisms and Catalysis. doi:10.1007/s11144-018-1490-1

27. Faskhutdinov, A. G., R. I. Faskhutdinova, I. A. Arefyev, and L. V. Enikeeva. 2019. Numerical simulation of the catalytic process of isomerization of pentane-hexane cut. Journal of Physics: Conference Series, 1368, 042016. doi:10.1088/1742-6596/1368/4/042016

28. Hayati, R., S. Z. Abghari, S. Sadighi, and M. Bayat. 2014. Development of a rule to maximize the research octane number RON of the isomerization product from light naphtha. Korean Journal of Chemical Engineering, 324, 629–635. doi:10.1007/s11814-014-0243-8

29. Chekantsev, N. V., M. S. Gyngazova, and E. D. Ivanchina. 2014. Mathematical modeling of light naphtha C5, C6 isomerization process. Chemical Engineering Journal, 238, 120-128. doi:10.1016/j.cej.2013.08.088

30. Li, C.L., and Z. L. Zhu. 1991. Network of n-hexane isomerization over Pt/Al2O3 and Pd/HM catalyst. Fuel Science and Technology International, 9(9), 1103–1121. doi:10.1080/08843759108942313

31. Koncsag, C.I., I.A. Tutun, and C. Safta. 2011. Study of C5/C6 isomerization on Pt/H-zeolite catalyst in industrial conditions, Ovidius Univ. Annal. Chem. 22(2), 102–106.

32. Chen, Z., J. Xu, Y. Fan, G. Shi, and X. Bao. 2015. Reaction mechanism and kinetic modeling of hydroisomerization and hydroaromatization of fluid catalytic cracking naphtha. Fuel Processing Technology, 130, 117–126. doi:10.1016/j.fuproc.2014.09.037

33. Ahmed, A. M., A. T. Jarullah, F. M. Abed, and I. M. Mujtaba. 2018. Modeling of an industrial naphtha isomerization reactor and development and assessment of a new isomerization process. Chemical Engineering Research and Design, 137, 33–46. doi:10.1016/j.cherd.2018.06.033

34. Ramos, M. J., A. de Lucas, V. Jiménez, P. Sánchez, and J. L. Valverde. 2008. Hydroisomerization of different refinery naphtha streams by using a Pt/BETA zeolite catalyst. Fuel Processing Technology, 898, 721–727. doi:10.1016/j.fuproc.2008.01.008

35. Pather, K., and D. Lokhat. 2014. Gas-phase Hydroisomerization of n-Hexane Over Pt/SO4-ZrO2: Kinetic Modeling and Reactor Simulation. Petroleum Science and Technology, 32(23), 2786–2794. doi:10.1080/10916466.2014.903969

36. Yasakova E.A., and A.V. Sitdikova, A.F. Achmetov. 2010. Tendency of isomerization process development in Russia and foreign countries, Oil and Gas Business, 1, 1-7.

Table 1. Kinetic parameters of proposed kinetic model.

	Pt/Mordinite		Pt/ZSM5		Pt/BETA	
Reaction	Pre-exponential factor (mol/gm.hr)	Activation energy (j/mol)	Pre-exponential factor (mol/gm.hr)	Activation energy (j/mol)	Pre-exponential factor (mol/gm.hr)	Activation energy (j/mol)
$\mathbf{n-C_4 \rightarrow i-C_4}$	2207.4	49388.66	21747.3	171502.5	2245.0	52074.39

$\mathbf{i-C_4 \rightarrow n-C_4}$	10309.4	147042.1	8591130.3	207866	17637.6	110654.4
$\mathbf{n-C_5 \rightarrow i-C_5}$	1740.9	38919.3	1186.4	24956.48	1719.2	27155.05
$\mathbf{i-C_5 \rightarrow n-C_5}$	3406828.2	198045.7	1959398.9	70596.66	2047318.2	74800.51
$\mathbf{n-C_5 \rightarrow CP+H_2}$	810687575.3	238674.6	235381364757.9	251056.6	3656496810.0	139487
$\mathbf{CP+H_2 \rightarrow n-C_5}$	7651.0	117083.5	3568065.1	218196.4	13141.3	93211.93
$\mathbf{MCP+H_2 \rightarrow 2-MP}$	769.5	58240	641.2	55111.53	1135.8	236851.5
$\mathbf{MCP+H_2 \rightarrow 3-MP}$	7822694421.0	255935.6	1471514106612.8	253218.7	9076467175.3	147312.5
$\mathbf{MCP \rightarrow CH}$	578.2	255464.3	376070.7	265755.1	932.7	196502.5
$\mathbf{CH \rightarrow MCP}$	772.1	51382.18	3557.9	62607.7	1202.4	49603.63
$\mathbf{B+3H_2 \rightarrow MCP}$	2831083.6	101229.1	1899242.6	76858.61	1918084.9	71600.34
$\mathbf{MCP \rightarrow B+3H_2}$	112222.8	215304.6	145299.5	202471.9	83185.9	147131.9
$\mathbf{B+3H_2 \rightarrow CH}$	5072.0	40757.19	210333.6	38358.82	8057.9	42987.34
$\mathbf{CH+H_2 \rightarrow n-C_6}$	21567.1	297038.1	23694.0	70360.6	39730.0	121717
$\mathbf{n-C_6 \rightarrow CH+H_2}$	13977478.8	182269.8	166832493.0	262646.6	4294870.9	230559.1
$\mathbf{n-C_6 \rightarrow 2-MP}$	27253.2	95610.42	1377151.5	100726.4	14051.0	66397.11
$\mathbf{2-MP \rightarrow n-C_6}$	10137521.1	293420.2	12649441191.3	244747.1	28335793.0	279009.9
$\mathbf{n-C_6 \rightarrow 3-MP}$	824.1	61157.76	6728.2	60220.17	741.3	49364.47
$\mathbf{3-MP \rightarrow n-C_6}$	178.0	167431.4	61216.9	257571.1	286.1	280288.4
$\mathbf{2-MP \rightarrow 2,3-DMB}$	6160.6	66495.93	88321.3	103685.6	16625.9	218332
$\mathbf{2,3-DMB \rightarrow 2-MP}$	3447714.6	219928.4	21562875.4	52509.79	3704234.0	92090.12
$\mathbf{3-MP \rightarrow 2,3-DMB}$	10226.7	79484.46	157457.9	70877.9	11001.7	39483.56
$\mathbf{2,3-DMB \rightarrow 3-MP}$	39292.3	256074.5	6177228.6	219216.4	49188.7	44669.45
$\mathbf{2-MP \rightarrow 3-MP}$	1137830.9	136823.4	76198640.4	129865.4	2480251.7	188261.3
$\mathbf{3-MP \rightarrow 2-MP}$	8081870.3	203592.9	146604449.2	161757.8	5797588.0	166461.8
$\mathbf{MCH+H_2 \rightarrow n-C_7}$	1078.7	209566.7	7500.5	176569.9	20308.8	75544.47
$\mathbf{n-C_7 \rightarrow 2-MH}$	304.5	55035.21	1261.9	48930.05	435.9	46041.93
$\mathbf{2-MH \rightarrow n-C_7}$	30434.9	226439.2	21607004.1	238654.3	30400.8	191250
$\mathbf{n-C_7 \rightarrow 3-MH}$	676455.5	96132.17	2251123.3	88621.6	2407536.4	89477.92
$\mathbf{3-MH \rightarrow n-C_7}$	21637.4	253301.3	23828.9	170859.5	58836.2	211627.7
$\mathbf{2-MH \rightarrow 2,2-DMP}$	4413222.5	185656.8	268426139.2	215525.8	13695453.7	111685.1
$\mathbf{2,2-DMP \rightarrow 2-MH}$	40360.1	199246.4	93734671.0	141361	147199.3	257200.7
$\mathbf{2-MH \rightarrow 2,3-DMP}$	15028.6	67085.39	2803840.8	234723.8	20336.5	66359.66
$\mathbf{2,3-DMP \rightarrow 2-MH}$	250812.4	101000.3	1452885283.6	114360.9	214128.8	245773.3
$\mathbf{2-MH \rightarrow 2,4-DMP}$	20441.0	73555.21	58473.8	71808.92	32692.6	64078.19
$\mathbf{2,4-DMP \rightarrow 2-MH}$	756739060.0	147525.9	5386626298.4	127919.8	1006909390.0	243416.1
$\mathbf{3-MH \rightarrow 2,3-DMP}$	830471.8	92446	43679229.7	100830.2	1975547.7	89258.07
$\mathbf{2,3-DMP \rightarrow 3-MH}$	104223068.7	203788.5	146099913.7	259023.9	66761904.5	299869.9
$\mathbf{3-MH \rightarrow 3,3-DMP}$	3521.5	63867.22	199338.1	114973.1	4728.3	64462.97
$\mathbf{3,3-DMP \rightarrow 3-MH}$	2084.6	188202.1	2062172.9	201870.5	2402.1	75434.98
$\mathbf{2,2-DMP \rightarrow 2,2,3-TMB}$	16347172.3	282595.1	27368952056.9	168405.2	14171819.8	147416.2
$\mathbf{2,2,3-TMB \rightarrow 2,2-DMP}$	65535.6	159441.7	2027373.5	220549.8	53210.2	29772.51
$\mathbf{2,3-DMP \rightarrow 2,2,3-TMB}$	8092.1	71065.96	494651.0	183665.3	5621.2	55642.47
$\mathbf{2,2,3-TMB \rightarrow 2,3-DMP}$	636205.0	86507.46	4769004.3	236197.5	117366.6	150890.8
$\mathbf{2,3-DMP \rightarrow 2,4-DMP}$	100510.0	73711.75	28683399.2	100983.3	192604.9	152049.3

$2,4-DMP \rightarrow 2,3-DMP$	77718490.6	139595.9	4993037202.5	164494.2	44823408.7	213149.4
$2,2-DMP \rightarrow 2,4-DMP$	5066564.1	241399	7465857.7	221308.7	3582145.6	131557.4
$2,4-DMP \rightarrow 2,2-DMP$	2888.6	57796.12	19477.2	275142.2	3297.7	49756.01
$2,2-DMP \rightarrow 1,1-DMCP+H_2$	6332.3	282022.5	448940.4	263213	5803.6	56642.38
$1,1-DMCP+H_2 \rightarrow 2,2-DMP$	954133.6	276453.7	3537026.1	279180.2	10249557.6	105852.3
$3,3-DMP \rightarrow 1,1-DMCP+H_2$	569.1	37870.76	818814.7	206423.2	4516.4	60073.64
$1,1-DMCP+H_2 \rightarrow 3,3-DMP$	30355.3	90228.07	5765874.4	129122.7	57149.9	207138.7
$2,4-DMP \rightarrow T1,3-DMCP+H_2$	1600.8	47511.17	3824.1	47977.91	1715.9	43228.52
$T1,3-DMCP+H_2 \rightarrow 2,4-DMP$	3791121.3	218746.9	27284699.5	107566.5	2143211.6	88753.04
$2,3-DMP \rightarrow T1,2-DMCP+H_2$	1581.1	51465.91	6365.1	55280.19	3844.4	54095.78
$T1,2-DMCP+H_2 \rightarrow 2,3-DMP$	24636.0	281135.3	13492923.3	104635.1	133895.9	80726.73
$2,3-DMP \rightarrow C1,2-DMCP+H_2$	727.9	51786.76	214019.2	88997.56	1027.6	48833.12
$C1,2-DMCP+H_2 \rightarrow 2,3-DMP$	2982.3	248327	14489.9	211787.2	2746.7	64086.92
$Tol+3H_2 \rightarrow MCH$	234.0	28247.26	126.0	25758.93	2547.3	30089.09
$MCH+H_2 \rightarrow 2-MH$	1806.9	57840.77	1806.6	57115.06	3629.1	56852.61
$MCH+H_2 \rightarrow 3-MH$	1365.6	63158.76	18724.4	75340.87	2139.6	262815.6
$2-MH \rightarrow 2M-1,5-Hexadiene+2H_2$	4611.0	70051.94	122493.2	164213.2	31094.0	93874.29
$2M-1,5-Hexadiene+2H_2 \rightarrow 2-MH$	1360345.2	104919	9480585.3	175936.2	910411.4	186911.2
$n-C_8 \rightarrow 2-MHe$	604769.1	92772.63	918483234.7	230621.5	774403.1	80686.89
$2-MHe \rightarrow n-C_8$	131737.9	261050.8	370476.3	78536.76	845636.5	225441.2
$n-C_8 \rightarrow 3-MHe$	37506228.5	122018.9	2960693017.4	271020.4	67946243.1	125039.3
$3-MHe \rightarrow n-C_8$	13864.7	222024	44961429.0	184882.5	56160.4	170646.4
$n-C_8 \rightarrow 4-MHe$	402.5	57740.21	2135.6	51815.96	646.7	46119.62
$4-MHe \rightarrow n-C_8$	3317922.7	237293.2	2060199.8	220450.4	3829956.6	295567.5
$2-MHe \rightarrow 3-MHe$	1789.9	55730.17	2528056.6	93607.45	2063.9	58141.47
$3-MHe \rightarrow 2-MHe$	44283568.9	197891.2	125015925.7	114285.5	64151673.0	113286.5
$2-MHe \rightarrow 2,2-DMH$	153.9	48130.99	220.2	44864.82	141.1	39122.61
$2,2-DMH \rightarrow 2-MHe$	108660.6	163062.4	50064496.3	136509.2	251286.4	161764.4
$2-MHe \rightarrow 2,3-DMH$	12962232.2	117342	66809330.4	133651.3	15121386.3	233670.2
$2,3-DMH \rightarrow 2-MHe$	12568139.9	207782.6	181099800940.8	164233.5	9743974.9	94582.25
$2-MHe \rightarrow 2,4-DMH$	211333.8	181451.5	2182558.3	93041.65	106935.1	221808.9
$2,4-DMH \rightarrow 2-MHe$	79774773.5	148460.4	306549869.8	118477	30503283.1	99020.72
$2-MHe \rightarrow 2,5-DMH$	29033.8	81377.18	2329919.3	109074.1	39027.0	67458.76
$2,5-DMH \rightarrow 2-MHe$	101490.3	275284.8	58384.7	225439.9	130933.3	179234
$3-MHe \rightarrow 3,3-DMH$	1907.7	65191.41	94824.0	82984.43	1191.6	58655.89
$3,3-DMH \rightarrow 3-MHe$	13593600.9	145725.5	437289121.0	238277.1	21043527.9	203013.6
$3-MHe \rightarrow 2,3-DMH$	14526766.2	106174.1	11491132939.6	224931.5	9300727.7	212464.2
$2,3-DMH \rightarrow 3-MHe$	262450.5	68999.36	1502914.5	90411.73	951681.7	93243.6
$3-MHe \rightarrow 3,4-DMH$	136165.9	80687.74	930412.5	85041.31	182115.6	78476.54
$3,4-DMH \rightarrow 3-MHe$	39396.0	245168.6	1625743.8	205420.9	18180.2	285855.9
$4-MHe \rightarrow 3,4-DMH$	263.9	52677.7	117.9	31023.02	258.9	34401.99
$3,4-DMH \rightarrow 4-MHe$	6513785.5	274588.2	5664379.6	215040	4619528.9	273297.9
$2,3-DMH \rightarrow T1,C2,4-TMCP+H_2$	11399718.4	142000.4	840532662.5	220308.7	16081782.4	219606.9
$T1,C2,4-TMCP+H_2 \rightarrow 2,3-DMH$	11612.9	65796.7	44368282.3	115401.9	11330.4	64292.04

$2,3-DMH \rightarrow T1,C2,3-TMCP+H_2$	7343831.4	228299.7	9191045676.3	167346.6	26296803.2	104772.3
$T1,C2,3-TMCP+H_2 \rightarrow 2,3-DMH$	7683.8	55829.85	4182.3	61547.14	7574.0	57225.19
$2-MHe \rightarrow 2-M,3-EP$	100993.7	192077.1	1966849.7	178125.8	177993.0	243999.5
$2-M,3-EP \rightarrow 2-MHe$	4489215.0	121961.5	1912938.3	103162.2	1296446.7	109040.1
$n-C_8 \rightarrow 3-EH$	517.5	48812.6	2371.5	45133.22	694.0	49385.35
$3-EH \rightarrow n-C_8$	842049.5	271103	668475.4	78939.84	1310310.5	104278.3
$2,4-DMH \rightarrow C1,3-DMCH+H_2$	9422123.2	137315.7	3288623.4	64907.97	5546349.1	217685.9
$C1,3-DMCH+H_2 \rightarrow 2,4-DMH$	456.1	48348.25	393.6	19091.32	452.3	34620.55
$2,5-DMH \rightarrow T1,4-DMCH+H_2$	1336915.8	227546	438767775.9	268549.8	3965814.1	271204.7
$T1,4-DMCH+H_2 \rightarrow 2,5-DMH$	6001.4	45601.42	4144.8	32779.61	11047.9	56705.84
$4-MHe \rightarrow t-1-M,3-ECP+H_2$	4383.9	72901.58	42605.2	80204.34	11200.2	85445.9
$t-1-M,3-ECP+H_2 \rightarrow 4-MHe$	560887.6	147672.7	21786318.3	157415.1	355563.7	242988.8
$3-EH \rightarrow t-1-M,3-ECP+H_2$	879594.5	243558	2407426.6	94527.42	829050.9	216486.5
$t-1-M,3-ECP+H_2 \rightarrow 3-EH$	268477829.6	236625.3	9949501714.6	131697.5	8077289581.4	143903
$4-MHe \rightarrow C-1-M,3-ECP+H_2$	8551695.5	144690.3	12840235.5	246857.4	8610134.6	216755
$C-1-M,3-ECP+H_2 \rightarrow 4-MHe$	2217.3	56921.5	103752.9	124874.1	14919.0	292024.6
$2,4-DMH \rightarrow C-1-M,3-ECP+H_2$	298.2	48409.57	349.0	52783.65	397.7	51441.05
$C-1-M,3-ECP+H_2 \rightarrow 2,4-DMH$	25019604.6	265954.1	5016455069.3	146096.1	86372421.5	145103
$4-MHe \rightarrow t-1-M,2-ECP+H_2$	2056.1	61307.64	6132.0	249402.1	1908.1	56801.03
$t-1-M,2-ECP+H_2 \rightarrow 4-MHe$	410136.5	214438.4	910152.0	80044.67	820256.6	95112.6
$3,4-DMH \rightarrow t-1-M,2-ECP+H_2$	33733288129.0	268483.5	274499847163.6	235853.3	14973022213.1	259410.9
$t-1-M,2-ECP+H_2 \rightarrow 3,4-DMH$	304058.9	117409.3	96178850.9	255580.1	626576.7	124052.9
$3-MHe \rightarrow t-1-M,1-ECP+H_2$	16068.6	161120.6	284839.3	215059.6	16033.8	295308.3
$t-1-M,1-ECP+H_2 \rightarrow 3-MHe$	2383.5	56135.87	2232.8	66072.2	2999.4	43066.06
$3-EH \rightarrow t-1-M,1-ECP+H_2$	53582.5	76858.36	201799.4	178143	42472.0	69493.64
$t-1-M,1-ECP+H_2 \rightarrow 3-EH$	280.5	41727.08	37647.6	78415.02	132.9	292883.5
$3-MHe \rightarrow T1,2-DMCH+H_2$	3232.4	59140.5	40558.1	66085.5	21562.0	74983.15
$T1,2-DMCH+H_2 \rightarrow 3-MHe$	686086.5	283592.6	15269394.9	197535.2	1295207.7	264571.1
$i-C_4+H_2 \rightarrow C_3+C_1$	1690641	196132.6	24260727	231389.9	2540150	194161.4
$i-C_4+H_2 \rightarrow 2C_2$	162031.2	297035.2	6547274	293912.5	549258.8	281795.4
$n-C_4+H_2 \rightarrow C_3+C_1$	4008.295	257541.9	16777.31	269274.9	2814.772	294919.9
$n-C_4+H_2 \rightarrow 2C_2$	4600965	282028.4	88233280	252315.2	10586270	211723.8
$i-C_5+H_2 \rightarrow i-C_4+C_1$	2.46E+08	188009	3.67E+08	235861	1.77E+08	295232.5
$i-C_5+H_2 \rightarrow n-C_4+C_1$	878587.9	187126.2	12213294	262505.7	1041682	198853.8
$i-C_5+H_2 \rightarrow C_3+C_2$	1233736	286586.4	3932985	176390.9	2652301	258559.7
$n-C_5+H_2 \rightarrow n-C_4+C_1$	33080985	200511	1.11E+10	260414.4	16565965	263757.4
$n-C_5+H_2 \rightarrow C_3+C_2$	1.46E+08	250828.5	1.82E+09	296320.8	2.78E+08	257569.2
$2,3-DMB+H_2 \rightarrow i-C_5+C_1$	3.48E+08	126256.5	2.29E+09	281178.7	1.56E+09	141206.7
$2,3-DMB+H_2 \rightarrow 2C_3$	2588.553	234741.7	781662	185564.7	5423.643	142906.6
$2-MP+H_2 \rightarrow i-C_5+C_1$	2245071	284035.8	6.24E+09	259445.6	21171233	109782.6
$2-MP+H_2 \rightarrow i-C_4+C_2$	2722977	247122.7	53138759	219132.6	5616477	225415.9
$2-MP+H_2 \rightarrow 2C_3$	1596808	271312.3	67971710	105921.4	1889252	92515.95
$3-MP+H_2 \rightarrow i-C_5+C_1$	1.55E+08	155480	7.12E+10	247299.3	2.56E+08	136528.9
$3-MP+H_2 \rightarrow n-C_5+C_1$	281.9328	297029.4	559.1454	218206.6	478.2296	215621.9

$3-MP+H_2 \rightarrow n-C_4+C_2$	58076.5	104228.2	1015323	285317.5	62650.35	216848.4
$n-C_6+H_2 \rightarrow n-C_4+C_2$	267588.1	101455.1	17419034	189310.1	157722.1	139800.2
$n-C_6+H_2 \rightarrow n-C_5+C_1$	3429.448	62457.46	34182.19	212690.6	7359.025	94298.26
$n-C_6+H_2 \rightarrow 2C_3$	9580.239	220500.3	9545.451	60991.78	12937.36	148105.6
$2,2-DMP+H_2 \rightarrow 2-MP+C_1$	15714.7	194955.3	172003.8	168499.5	18518.51	243198.6
$2,2-DMP+H_2 \rightarrow i-C_5+C_2$	1587350	268263.9	6.16E+08	255914	1890219	260643.1
$2,2-DMP+H_2 \rightarrow i-C_4+C_3$	5996256	185043.7	7.29E+10	198413.8	6539617	90243.85
$2,4-DMP+H_2 \rightarrow 2-MP+C_1$	393756.9	279056.5	36469534	263644	318841.3	289387.2
$2,4-DMP+H_2 \rightarrow i-C_4+C_3$	2688994	132941	24172312	91592.12	2599729	82599.17
$2,2,3-TMB+H_2 \rightarrow 2,3-DMB+C_1$	13472.51	172327.1	85857.51	146557.8	57653.07	136375.3
$2,2,3-TMB+H_2 \rightarrow i-C_4+C_3$	8003846	254856.1	4.87E+08	119256.6	2171458	78749.11
$3,3-DMP+H_2 \rightarrow 2-MP+C_1$	69932138	281213.5	6.75E+08	257064.7	57073105	274030.3
$3,3-DMP+H_2 \rightarrow 3-MP+C_1$	2256500	259029.1	12363850	207730.3	4219839	285240.4
$3,3-DMP+H_2 \rightarrow n-C_4+C_3$	6095615	173999.9	1.28E+10	149696.6	23835470	104109.4
$2-MH+H_2 \rightarrow n-C_6+C_1$	277.0855	270679.3	49.62406	194974.9	844.4634	140603
$2-MH+H_2 \rightarrow 2-MP+C_1$	160.7936	244848.8	740.2316	274919.3	351.5008	161245.3
$2-MH+H_2 \rightarrow i-C_4+C_3$	757.514	50139.65	878.0012	41382.88	395.4225	48108.39
$2,3-DMP+H_2 \rightarrow 2-MP+C_1$	42469.31	245586.6	2336550	243525.9	111304.9	296188.7
$2,3-DMP+H_2 \rightarrow 3-MP+C_1$	61519.85	234571.2	776838	229788.1	50185.42	292821.6
$2,3-DMP+H_2 \rightarrow 2,3-DMB+C_1$	11540.8	299487.8	450450.2	152560.3	129141.1	288704.5
$2,3-DMP+H_2 \rightarrow n-C_4+C_3$	4566492	106013.5	1.96E+09	201701	22320647	95623.51
$3-MH+H_2 \rightarrow n-C_6+C_1$	33046.7	198785.3	35760053	200373.5	82404.16	246762.4
$3-MH+H_2 \rightarrow 3-MP+C_1$	33392.61	264947.8	16097837	251202.2	21497.86	172550.8
$3-MH+H_2 \rightarrow i-C_5+C_2$	3.84E+08	198899.7	1E+11	264883	1.52E+09	147850.6
$3-MH+H_2 \rightarrow n-C_4+C_3$	78432.26	83607.5	113409.2	76081.45	263664.3	81349.62
$n-C_7+H_2 \rightarrow n-C_4+C_3$	46997.91	77697.42	47673887	116631.8	6893.192	72839.06
$n-C_7+H_2 \rightarrow n-C_5+C_2$	4272668	162281.1	17189655	254358.7	5756367	258604.9
$n-C_7+H_2 \rightarrow n-C_6+C_1$	2120.947	159202.5	154497.4	278247.7	3864.036	219848.3
$2,2-DMH+H_2 \rightarrow 2-MH+C_1$	30955.45	228645.6	3288846	249892.2	49884.82	172950.7
$2,2-DMH+H_2 \rightarrow 2,2-DMP+C_1$	56711049	289287.2	61846813	208062.6	95977896	245065.7
$2,2-DMH+H_2 \rightarrow i-C_4+n-C_4$	253.7506	50338.56	17363.32	71895.26	178.7112	34419.41
$2,5-DMH+H_2 \rightarrow 2-MH+C_1$	25726.99	297965.5	521210.3	256690.4	22278.39	237329.9
$2,5-DMH+H_2 \rightarrow 2i-C_4$	31276.06	72979.85	39447.77	70336.52	30566.23	60065.49
$2,5-DMH+H_2 \rightarrow i-C_5+C_3$	13313.2	169608.2	330266.5	191769.6	22728.38	176440.6
$2,4-DMH+H_2 \rightarrow 2,4-MP+C_1$	1.04E+08	217927	5.43E+09	248558.8	69824109	194512.4
$2,4-DMH+H_2 \rightarrow 2-MH+C_1$	4338.816	237831.7	894998.1	165856.3	1326.421	275683.2
$2,4-DMH+H_2 \rightarrow 2-MP+C_2$	16674552	260356.1	1.88E+09	239065.7	45988908	202565.5
$2,4-DMH+H_2 \rightarrow n-C_4+C_3$	251229.6	112735.1	7.97E+09	139528.4	334417.6	204823.8
$3,3-DMH+H_2 \rightarrow 3-MH+C_1$	238175.9	173175.5	12863588	241351.2	248163.5	259247.5
$3,3-DMH+H_2 \rightarrow 3,3-DMP+C_1$	26710.01	210772.3	393007.1	173458.7	62018.75	173789.7
$3,3-DMH+H_2 \rightarrow i-C_5+C_3$	8723.263	87145.19	86762.74	166092.8	7074.458	55046.44
$2,3,4-TMP+H_2 \rightarrow 2,3-DMP+C_1$	533006.3	167374	470131.3	211999.4	350986.8	189680.1
$2,3,4-TMP+H_2 \rightarrow 2,4-DMP+C_1$	92632.98	228795.7	2267546	212364.5	311959	284566.8
$2,3,4-TMP+H_2 \rightarrow i-C_5+C_3$	1907794	176994.8	3329642	98055.91	4885747	92143.59

$\mathbf{2,3-DMH+H_2 \rightarrow 2-MH+C_1}$	11029.71	252666.4	344822.8	269141	5171.068	288546.9
$\mathbf{2,3-DMH+H_2 \rightarrow 3-MH+C_1}$	29982.15	270086.2	2349564	214988.7	134418	186710.5
$\mathbf{2,3-DMH+H_2 \rightarrow 2,3-DMP+C_1}$	2565085	227522.4	89497131	204768.3	3899594	133180.9
$\mathbf{2,3-DMH+H_2 \rightarrow 2,3-DMB+C_2}$	961522.2	187241.9	7755021	269077.9	2828269	254735.3
$\mathbf{2,3-DMH+H_2 \rightarrow i-C_4+C_3}$	41313.46	187819.4	32904.88	77716.26	19090.57	188235.4
$\mathbf{2-M,3-EP+H_2 \rightarrow 2,3-DMP+C_1}$	1.72E+08	186457.8	5.94E+09	209548.8	6.83E+08	245126.2
$\mathbf{2-M,3-EP+H_2 \rightarrow 2-MP+C_2}$	858775.6	277160.5	9670697	262526.9	544344.5	208555.8
$\mathbf{2-M,3-EP+H_2 \rightarrow n-C_5+C_3}$	800057.8	123645.1	188147.1	83238.03	338816.9	80501.03
$\mathbf{2-MHe+H_2 \rightarrow n-C_7+C_1}$	3.08E+09	241773	1.86E+11	282752.6	7.65E+09	297159.9
$\mathbf{2-MHe+H_2 \rightarrow 2-MH+C_1}$	48382.11	180940.6	24164203	229397.7	165861.2	236204.4
$\mathbf{2-MHe+H_2 \rightarrow 2-MP+C_2}$	377967.1	175849.2	141045.3	184948.2	658553.6	288608.8
$\mathbf{2-MHe+H_2 \rightarrow i-C_5+C_3}$	138963.6	149829.4	82855.41	74829.31	91841.89	81433.98
$\mathbf{2-MHe+H_2 \rightarrow 2n-C_4}$	71640.72	82912.09	63187.85	78378.04	59714.6	70526
$\mathbf{3-MHe+H_2 \rightarrow n-C_7+C_1}$	33102.25	251605.9	488815.2	161329.2	28688.59	287664
$\mathbf{3-MHe+H_2 \rightarrow 3-MH+C_1}$	23311.07	279817.7	949351.1	241717.6	41816.03	187702.8
$\mathbf{3-MHe+H_2 \rightarrow 3-MP+C_2}$	7734768	177937.3	1.44E+08	217603.7	15148436	295267.1
$\mathbf{3-MHe+H_2 \rightarrow i-C_5+C_3}$	3559.333	213150.2	7080904	128078.8	22144.58	245328.4
$\mathbf{3-MHe+H_2 \rightarrow 2n-C_4}$	9676.93	69620.51	239844.3	191437.4	27210.38	80621.88
$\mathbf{4-MHe+H_2 \rightarrow n-C_7+C_1}$	37855.21	261996.9	2479651	280446.8	154601.9	209120.3
$\mathbf{4-MHe+H_2 \rightarrow 3-MH+C_1}$	4.18E+08	283601.1	8.1E+10	256612.8	7.75E+08	251344.8
$\mathbf{4-MHe+H_2 \rightarrow 2-MP+C_2}$	20050101	235013.6	1.63E+08	192294.9	1.35E+08	288120.9
$\mathbf{4-MHe+H_2 \rightarrow n-C_5+C_3}$	529810.7	238362.9	1207222	92062.65	1672638	297727.8
$\mathbf{3,4-DMH+H_2 \rightarrow 3-MH+C_1}$	13870844	256827.5	1.98E+08	238696.5	14512161	256787.5
$\mathbf{3,4-DMH+H_2 \rightarrow 2,3-DMP+C_1}$	1838.596	227050.3	173544.5	153731	4782.8	237213.7
$\mathbf{3,4-DMH+H_2 \rightarrow 3-MP+C_2}$	30164420	299066.5	4.01E+10	291232.7	1.47E+08	283552.5
$\mathbf{3,4-DMH+H_2 \rightarrow 2n-C_4}$	2564.309	47673.61	3896.75	43469.15	2988.633	46738.68
$\mathbf{n-C_8+H_2 \rightarrow n-C_7+C_1}$	1708426	296173.2	33116416	253055.2	1133586	241142.4
$\mathbf{n-C_8+H_2 \rightarrow n-C_6+C_2}$	640593.6	296686.1	5672394	168707.4	1415853	298218.1
$\mathbf{n-C_8+H_2 \rightarrow n-C_5+C_3}$	7598197	207804.1	3384682	101156.4	7288574	239512.7
$\mathbf{n-C_8+H_2 \rightarrow 2n-C_4}$	3564.534	68427.9	6582.37	60805.28	12682.08	196860.5

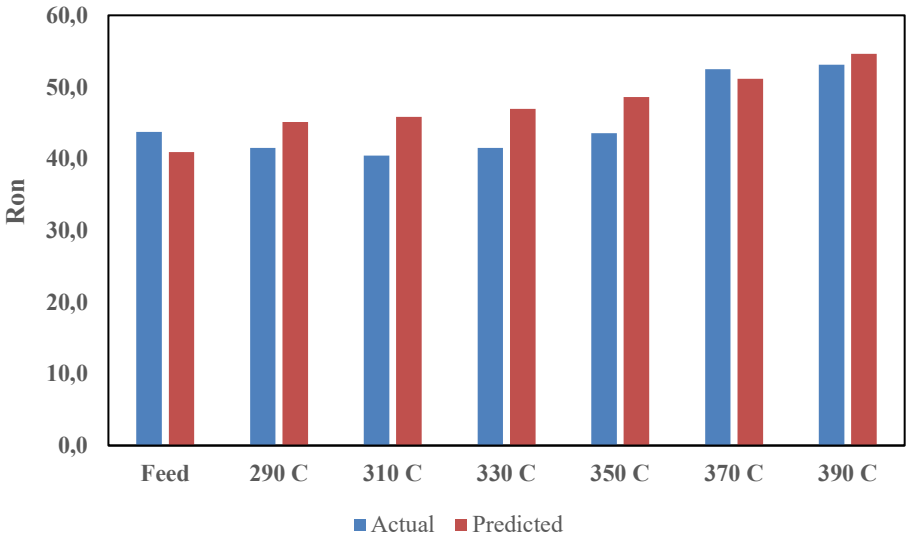

(a) Pt/Mordinite

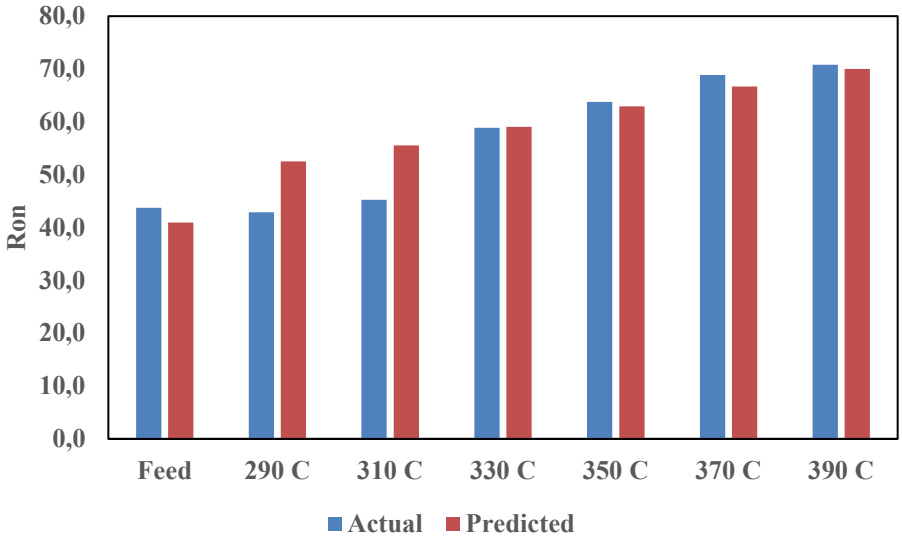

(b) Pt/ZSM5

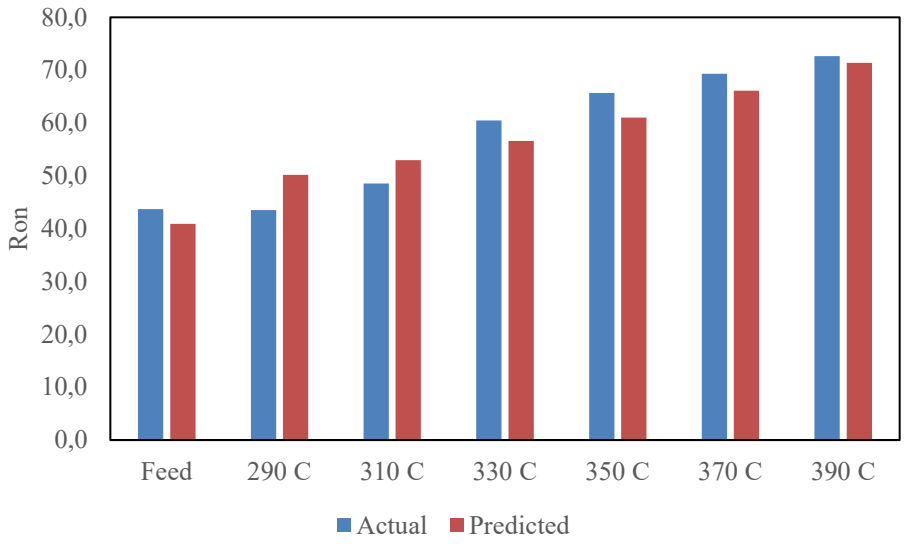

(c) Pt/BETA

Figure 1. Compression between actual and predicted research octane number (RON).

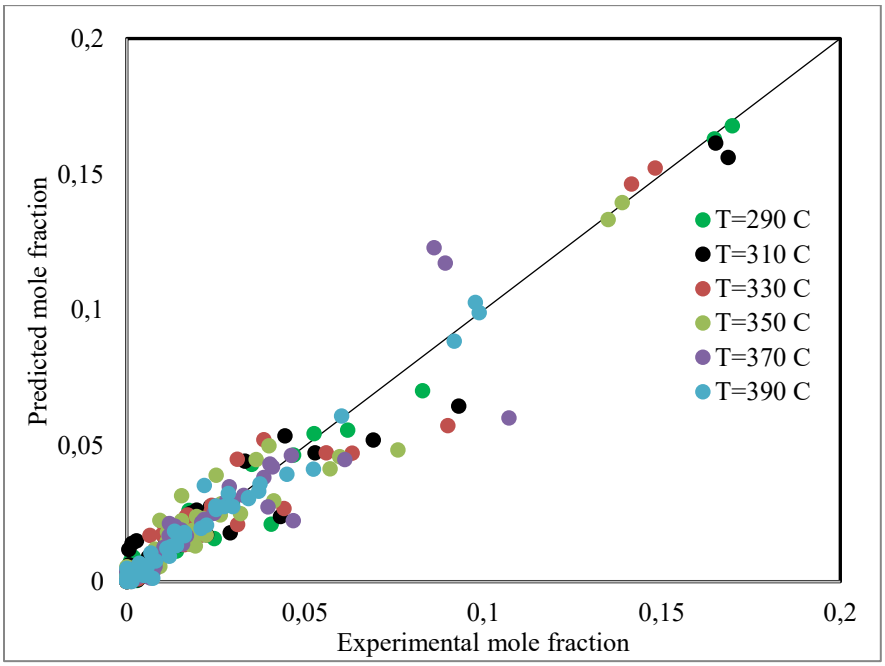

(a) Pt/Mordinite

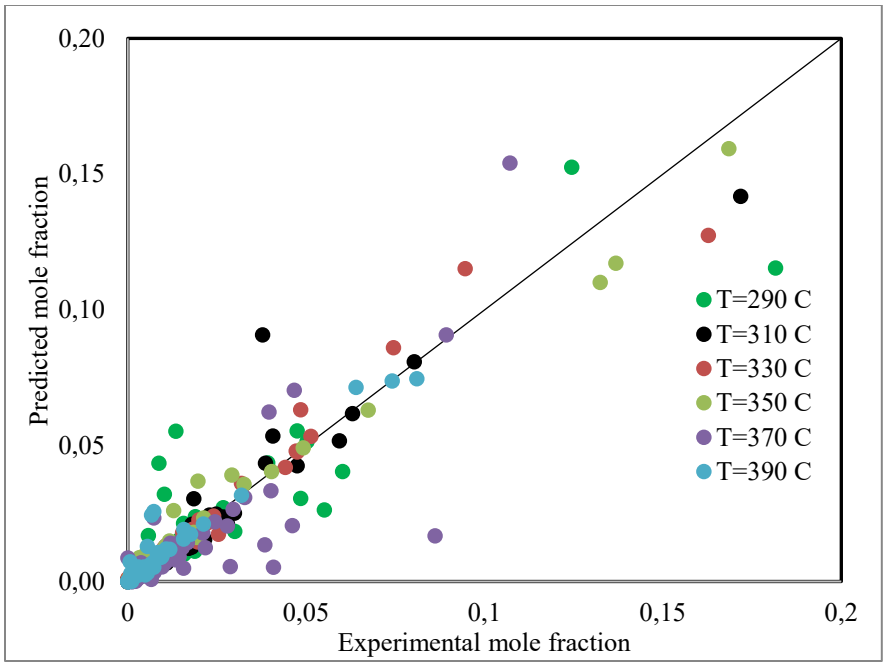

(b) Pt/ZSM5

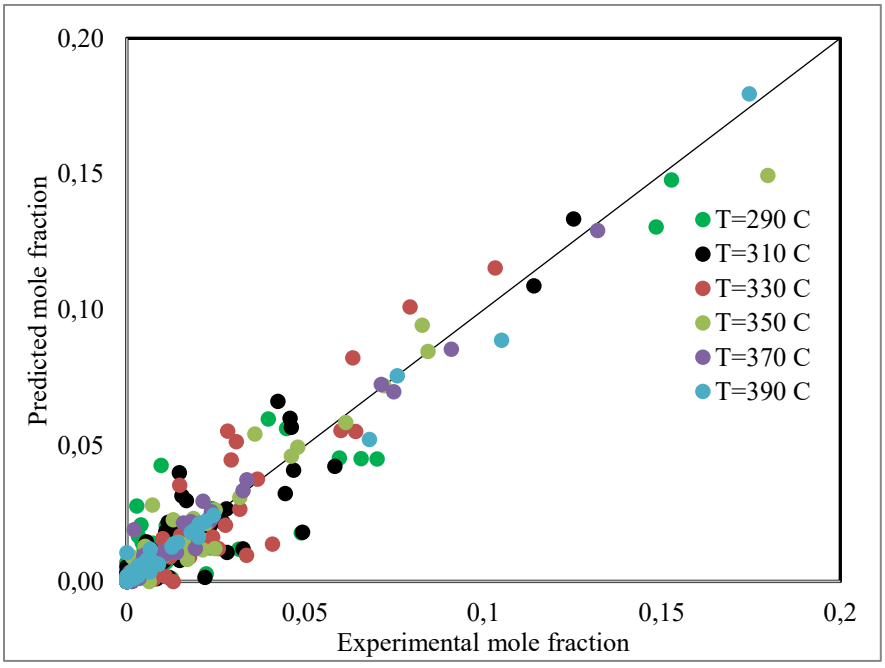

(c) Pt/BETA

Figure 2. Compression between actual and predicted composition.

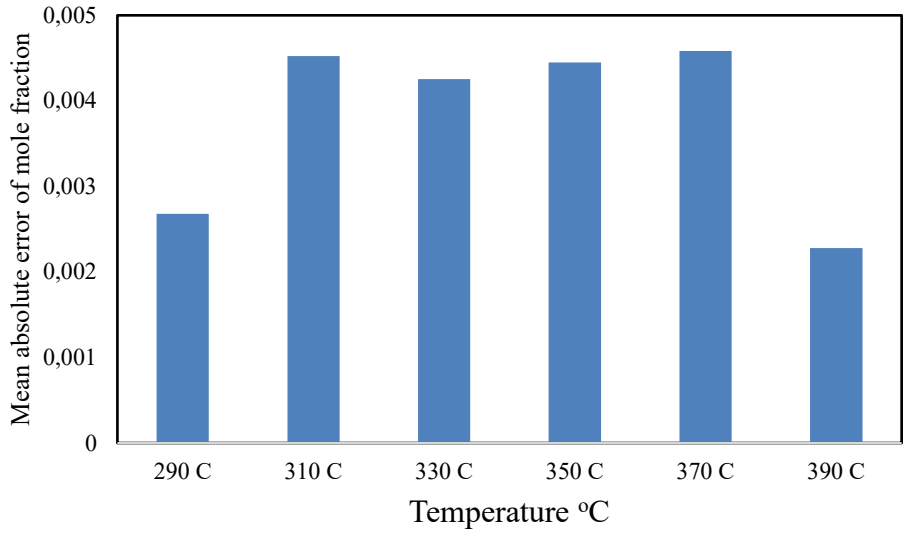

(a) Pt/Mordinite

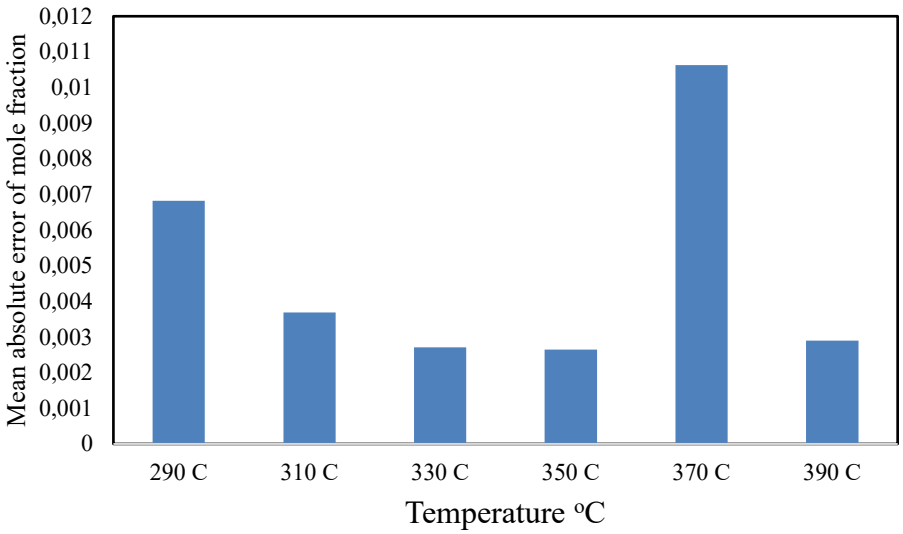

(b) Pt/ZSM5

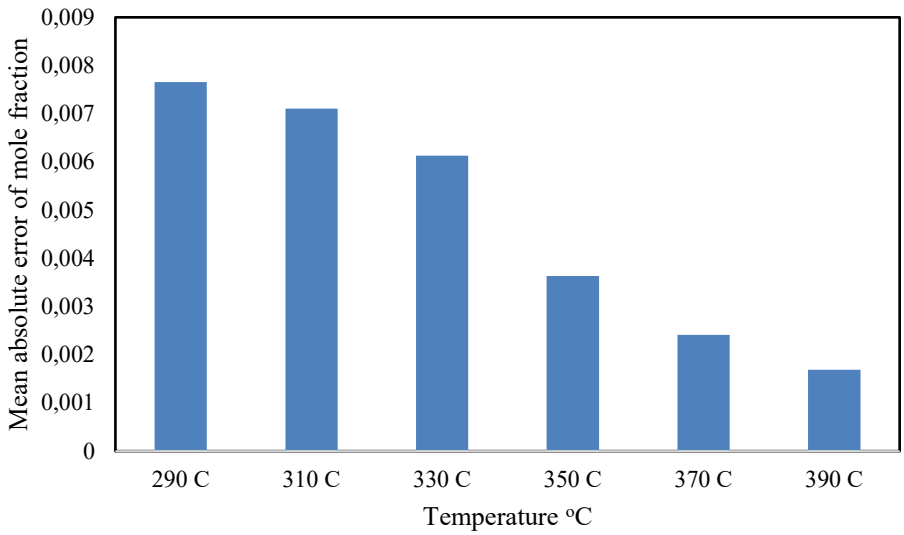

(c) Pt/BETA

(d) Figure 3. Compression between actual and predicted composition at different temperature.